Contribution from the Dipartimento di Chimica Inorganica, Metallorganica ed Analitica and Dipartimento di Chimica Organica, University of Padova, Padova, Italy, and Istituto di Chimica Generale ed Inorganica, University of Torino, Torino, Italy

The Alkyne–Cluster Interaction: Structural, Theoretical, and Spectroscopic Study on the Parallel μ_3-η^2 Bonding Mode in Trinuclear Carbonyl Clusters of Ruthenium and Osmium

S. Aime,*[1a] R. Bertoncello,[1b] V. Busetti,[1c] R. Gobetto,[1a] G. Granozzi,*[1b] and D. Osella[1a]

Received October 28, 1985

The parallel μ_3-η^2 alkyne–cluster interaction in compounds of formula $H_2M_3(CO)_9(RC_2R')$ (M = Ru, Os) has been studied by means of X-ray diffraction, ^1H and ^{13}C VT (variable temperature) NMR and UV-PES spectroscopy, and CNDO theoretical techniques. Crystals of $H_2Os_3(CO)_9(CH_3C_2CH_3)$ belong to the monoclinic space group $P2_1/n$ with unit cell dimensions of a = 14.538 (4) Å, b = 13.004 (4) Å, c = 9.817 (3) Å, β = 100.17 (5)°, and Z = 4. Full-matrix least-squares refinement converged to R = 4.95% for 3223 unique reflections. Relevant interatomic distances (Å): Os(1)–Os(2) = 3.016 (1), Os(1)–Os(3) = 2.763 (1), Os(2)–Os(3) = 2.858 (1), C(42)–C(43) = 1.434 (36), Os(1)–C(42) = 2.067 (24), Os(2)–C(43) = 2.198 (26), Os(3)–C(42) = 2.364 (28), Os(3)–C(43) = 2.263 (27). The small differences observed between the Os(1)–C(42) and Os(2)–C(43) distances are thought to reflect the charge imbalance on the metal atoms. The lowest energy dynamic process observed in the ^{13}C NMR spectra is consistent with an oscillatory motion of the alkyne and of the hydride bridging the Os(1)–Os(2) edge (H_a) coupled with the edge hopping of the second hydride (H_b). Subtle electronic changes induced by different substituents on the alkyne cause remarkable differences in the $^2J_{C,H}$ coupling pattern between H_a and CO ligands. The results of CNDO calculations have been used for the interpretation of the UV-PE spectra and for discussion of the bonding scheme of the studied molecules.

Introduction

Alkynes chemisorbed on transition-metal surfaces give rise to strong multicentered interactions with significant rehybridization of the acetylenic carbon atoms and formation of strong carbon–metal σ bonds.[2] Similar interactions are present also in several alkyne–cluster compounds, which can be envisaged as reasonable models of chemisorbed species on metallic surfaces. This cluster–surface analogy[3] may be examined by molecular spectroscopic techniques.

In previous studies we have reported NMR (^{13}C and ^1H), UV photoelectron spectroscopy (UV-PES), and theoretical results on the μ_2-η^2, μ_3-$\eta^2(\perp)$, and μ_4-η^2 alkyne–cluster bonding modes.[4]

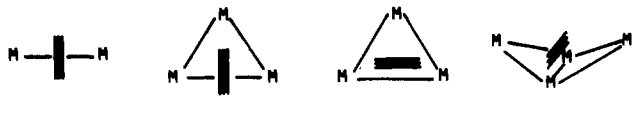

These studies indicated that the cluster–alkyne back-donation interactions play a major role in the alkyne rehybridization; the subtle balance in the alkyne–cluster donation and back-donation is strongly dependent upon the coordination mode.

Within the class of trinuclear alkyne–cluster compounds, geometry **B** has been recognized only in $Fe_3(CO)_9(RC_2R)$[5] and three heterometallic derivatives.[4c,6] Coordination mode **C** is more common, having been found in $Os_3(CO)_{10}(RC_2R)$ and $H_2M_3(CO)_9(RC_2R)$ (M = Ru, Os)[7] as well as in several heterometallic alkyne–cluster compounds.[6]

In the polyhedron skeletal electron pair (PSEP) theory,[8] form **B** can be viewed as a closo trigonal bipyramid (46-e unsaturated cluster) while form **C** can be viewed as a nido octahedron (48-e saturated cluster), and the increase of one skeletal electron pair should cause **B** → **C** interconversion. The same behavior has been predicted by Schilling and Hoffmann[9] on the basis of extended Hückel theoretical (EHT) considerations and confirmed in a recent paper by other authors.[10] Actually, the electrochemical behavior of $Fe_3(CO)_9(EtC_2Et)$[11] supports the occurrence of a reversible **B** ⇄ **C** interconversion via a 2-e redox process.

Within geometry of type **C**, the solid-state structures of 48-e MM'_2 heterometallic alkyne–cluster compounds have shown that both symmetrical (alkyne parallel to M–M) (i.e. $FeCo_2(CO)_9(RC_2R)$[12] and $FeNi_2(CO)_3(\eta^5\text{-}C_5H_5)_2(RC_2R)$[13]) and asymmetrical structures (alkyne parallel to M–M') (i.e. $RuCo_2(CO)_9(RC_2R)$[14]) can occur. Furthermore, in the case $W_2Os(CO)_7(\eta^5\text{-}C_5H_5)_2(RC_2R)$ both the possible rotamers are present in the unit cell.[15] It is noteworthy that all the asymmetrical structures show "semibridging" carbonyls, which redistribute electron density from electron-rich to electron-poor metal atoms.

The existence of different alkyne orientations led Schilling and Hoffmann to suggest that the μ_3-acetylenic moiety can be fluxional and a series of possible rearrangement pathways have been proposed.[16] The dynamic behavior of $H_2M_3(CO)_9(\mu_3\text{-}\eta^2(\|)\text{-alkyne})$ complexes (M = Ru, Os) has been studied by Deeming,[17] and several distinct fluxional processes have been proposed to occur: (a) transfer of a hydride ligand across the unbridged M–M bonds; (b) axial–equatorial CO exchange at each $M(CO)_3$ unit; (c)

(1) (a) University of Torino. (b) Dipartimento di Chimica Inorganica, Metallorganica ed Analitica, University of Padova. (c) Dipartimento di Chimica Organica, University of Padova.
(2) For a general survey on this topic see: (a) Muetterties, E. L. *Angew. Chem., Int. Ed. Engl.* **1978**, *17*, 545. (b) Ozin, G. A.; McIntosh, D. F.; Power, W. J.; Messmer, R. P. *Inorg. Chem.* **1981**, *20*, 1782. (c) Geurts, P.; Van Der Avoird, A. *Surf. Sci.* **1981**, *103*, 431 and references cited therein.
(3) (a) Ugo, R. *Catal. Rev.* **1975**, *11*, 225. (b) Muetterties, E. L.; Rhodin, T. N.; Band, E.; Brucker, C. F.; Pretzer, W. R. *Chem. Rev.* **1979**, *79*, 91.
(4) (a) Casarin, M.; Ajó, D.; Granozzi, G.; Tondello, E. *J. Chem. Soc., Dalton Trans.* **1983**, 869. (b) Granozzi, G.; Tondello, E.; Casarin, M.; Aime, S.; Osella, D. *Organometallics* **1983**, *2*, 430. (c) Busetti, V.; Granozzi, G.; Aime, S.; Gobetto, R.; Osella, D. *Organometallics* **1984**, *3*, 1510. (d) Granozzi, G.; Bertoncello, R.; Acampora, M.; Ajó, D.; Osella, D.; Aime, S. *J. Organomet. Chem.* **1983**, *244*, 383. (e) Granozzi, G.; Tondello, E.; Bertoncello, R.; Aime, S.; Osella, D. *Inorg. Chem.* **1983**, *22*, 744.
(5) Blount, J. F.; Dahl, L. F.; Hoogzand, C.; Hubel, W. J. *J. Am. Chem. Soc.* **1966**, *88*, 292.
(6) For a recent review see: Sappa, E.; Tiripicchio, A.; Braunstein, P. *Chem. Rev.* **1983**, *83*, 203.
(7) (a) Deeming, A. J.; Hasso, S.; Underhill, M. *J. Chem. Soc., Dalton Trans.* **1975**, 1614. (b) Evans, J.; McNulty, S. *J. Chem. Soc., Dalton Trans.* **1981**, 2017 and references therein.
(8) Mingos, D. M. P. *Acc. Chem. Res.* **1984**, *17*, 311 and references therein.
(9) Schilling, B. E. R.; Hoffmann, R. *J. Am. Chem. Soc.* **1979**, *101*, 3456.
(10) Halet, J. F.; Saillard, J. Y.; Lissillour, R.; McGlinchey, M. J.; Jaouen, G. *Inorg. Chem.* **1985**, *24*, 218.
(11) Zanello, P.; Osella, D., personal communication.
(12) Aime, S.; Milone, L.; Osella, D.; Tiripicchio, A.; Manotti-Lanfredi, A. M. *Inorg. Chem.* **1982**, *21*, 501.
(13) Sappa, E.; Manotti-Lanfredi, A. M.; Tiripicchio, A. *J. Organomet. Chem.* **1981**, *221*, 93.
(14) Braunstein, P.; Rose, J.; Bars, O. *J. Organomet. Chem.* **1983**, *252*, C101.
(15) Churchill, M. R.; Bueno, C.; Wasserman, H. J. *Inorg. Chem.* **1982**, *21*, 640.
(16) Schilling, B. E. R.; Hoffmann, R. *Acta Chem. Scand., Ser. B* **1979**, *B33*, 231.
(17) Deeming, A. J. *J. Organomet. Chem.* **1978**, *150*, 123.

0020-1669/86/1325-4004$01.50/0

unrestricted hydride migration; (d) alkyne rotation over the metal triangle, probably through 60° steps.

On the basis of these interesting features associated with coordination mode **C**, a detailed structural (X-ray diffraction) and spectroscopic (NMR, UV-PES) study on $H_2M_3(CO)_9$(alkyne) (M = Ru, Os) has been undertaken. A theoretical approach based on CNDO semiempirical calculations, which was recently shown to be accurate in discussing PE data of similar cluster compounds,[4] has been adopted in order to obtain a deeper insight into the bonding scheme of the title compound and to account for the differences between **B** and **C** type arrangements.

Experimental Section

The compounds $H_2Os_3(CO)_9(MeC_2Me)$[7a] (**1**), $H_2Ru_3(CO)_9(MeC_2Me)$[18a] (**2**), $H_2Ru_3(CO)_9(MeC_2Et)$[18b] (**3**), $H_2Ru_3(CO)_9(EtC_2Et)$[18b] (**4**), and $H_2Ru_3(CO)_9(MeC_2Pr)$[18b] (**5**) were prepared according to literature methods, and their purity was checked by IR and mass spectroscopies. **4** and **5** (obtained by hydrogenation of $H_2Ru_3(CO)_9(EtC{=}C{=}C(H)Me)$ in cyclohexane at reflux for 3 h) could not be separated by thin-layer chromatography, and therefore their PE and NMR spectra were recorded on their mixture. The relative ratio of **4** to **5** is 3:2, as established from ^{13}C NMR spectra of the organic ligands. ^{13}C NMR data for **4** (ppm): CH_3, 19.3 (q); CH_2, 40.8 (t); C_{ac}, 162.8. ^{13}C NMR data for **5** (ppm): CH_3, 14.1 (q); CH_2, 26.3 (t); CH_2, 34.7 (t); C_{ac}, 150.7; C_{ac}, 164.6.

^1H and ^{13}C NMR spectra were recorded on a JEOL GX 270/89 instrument. Chemical shifts are reported downfield positive with respect to $SiMe_4$. The samples used for ^{13}C NMR spectroscopy were synthesized by using the starting $M_3(CO)_{12}$ clusters (M = Ru, Os) enriched in ^{13}CO. The conditions for ^{13}CO enrichment are the following. (a) $Ru_3(CO)_{12}$: 150 mg was dissolved in 80 mL of cyclohexane and sealed in vial (volume 160 mL) under ^{13}CO atmosphere (about 150 Torr); the sealed vial was then heated at +50 °C for 4 days. (b) $Os_3(CO)_{12}$: the quantities and the procedure were the same as for $Ru_3(CO)_{12}$ except for the temperature (100 °C), time (2 days), and solvent (*n*-octane).

He I (21.217 eV) and He II (40.814 eV) gas-phase photoelectron spectra were recorded on a Perkin-Elmer PS-18 spectrometer modified for He II measurements by inclusion of a hollow-cathode discharge lamp, which gives a high photon flux at He II wavelengths (Helectros Developments). A heated-inlet probe system was adopted at 82–90 °C for compound **1** and at 55–60 °C for compound **2**. The spectrometer was connected on-line with a Minc-23 computer (Digital Equipment) by an interface built in our laboratory. Data acquisition was carried out by several sweeps (four to six) over 500 distinct channels. Typical sweep time amounts to 5 min. The ionization energy (IE) scale was calibrated by reference to peaks due to admixed inert gases (Xe, Ar) and to the He $1s^{-1}$ self-ionization.

Quantum-mechanical calculations were performed by a version of the CNDO method[19] suitable for transition-metal complexes. Fe and Ru semiempirical parameters were obtained[19] from atomic spectroscopic data whereas the C, O, and H parameters are Pople's standard ones.[20] Gross atomic charges and bond overlap populations (OPs) were obtained by Mulliken's population analysis[21] of the deorthogonalized[22] eigenvectors.

X-ray Analysis: $H_2Os_3(CO)_9(CH_3C_2CH_3)$ (**1**); monoclinic, space group $P2_1/n$, a = 14.538 (4) Å, b = 13.004 (4) Å, c = 9.817 (3) Å, β = 100.17 (5)°, V = 1826.8 (9) Å^3; D_c = 3.195 g·cm^{-3}, D_m = 3.19 g·cm^{-3}, $\mu_{Mo\,K\alpha}$ = 208.9 cm^{-1}, M_r = 878.80; Z = 4; $F(000)$ = 1544.

A very thin needle-shaped crystal, pale green-yellow in color, of dimensions 0.011 × 0.012 × 0.055 mm was used for data collection on a Philips PW 1100 four-circle diffractometer (Mo Kα radiation monochromated by a graphite plate, θ–2θ scan mode, scan width 1.0° at a speed of 0.02° s^{-1}, background measured for 10 s at each extremity, 2° < 2θ < 50°). Three standard intensity and orientation reflections were measured at 3-h intervals; no decomposition of the crystal was noticed during data collection. Of 3223 unique reflections, 1981 had $I \geq 2.5\sigma(I)$, and their intensities were corrected for Lorentz and polarization factors; an empirical absorption correction from a ψ scan of (602) reflection was also applied, minimum and maximum values 1.05 and 1.25, respectively; R_{int} = 2.62%. Heavy-atom positions were derived by Patterson methods; a F_o Fourier synthesis calculated with only their contributions revealed all carbon and oxygen atoms. Positional and anisotropic thermal parameters of the non-hydrogen atoms were refined by a full-matrix least-squares program with unitary weights; refinement converged to R = 4.95%. Atomic scattering factors were derived from ref 23, and

Table I. Atomic Coordinates and Equivalent Temperature Factors (Å^2)[a] of **1**

	x	y	z	B_{eq}
Os(1)	0.38421 (7)	0.23698 (8)	0.06206 (9)	2.67 (3)
Os(2)	0.32374 (7)	0.28367 (8)	0.33396 (9)	2.75 (2)
Os(3)	0.50284 (7)	0.33603 (8)	0.27233 (9)	2.61 (2)
C(11)	0.4744 (16)	0.2246 (18)	−0.0532 (22)	2.7 (6)
O(11)	0.5298 (13)	0.2186 (16)	−0.1249 (19)	4.9 (6)
C(12)	0.3144 (17)	0.3503 (23)	−0.0461 (28)	3.6 (8)
O(12)	0.2811 (16)	0.4201 (18)	−0.1094 (21)	5.9 (7)
C(13)	0.3157 (20)	0.1219 (20)	−0.0216 (30)	4.2 (8)
O(13)	0.2777 (14)	0.0502 (16)	−0.0729 (24)	5.8 (7)
C(21)	0.3477 (17)	0.3227 (23)	0.5277 (30)	4.1 (7)
O(21)	0.3635 (15)	0.3508 (21)	0.6365 (22)	6.8 (8)
C(22)	0.2197 (19)	0.3856 (19)	0.2897 (31)	4.1 (8)
O(22)	0.1616 (16)	0.4350 (19)	0.2534 (25)	6.7 (9)
C(23)	0.2467 (20)	0.1659 (21)	0.3684 (27)	4.2 (8)
O(23)	0.2097 (17)	0.0974 (17)	0.3826 (24)	7.0 (8)
C(31)	0.5624 (18)	0.3760 (22)	0.4557 (24)	3.5 (8)
O(31)	0.5945 (16)	0.3970 (19)	0.5639 (21)	6.6 (8)
C(32)	0.4965 (16)	0.4642 (20)	0.1857 (23)	2.7 (6)
O(32)	0.4947 (14)	0.5496 (16)	0.1396 (22)	5.3 (7)
C(33)	0.6173 (21)	0.3013 (21)	0.2131 (28)	4.1 (8)
O(33)	0.6824 (14)	0.2816 (19)	0.1700 (22)	6.4 (7)
C(41)	0.5418 (19)	0.0807 (20)	0.2175 (34)	4.8 (9)
C(42)	0.4673 (17)	0.1610 (22)	0.2236 (24)	3.5 (7)
C(43)	0.4512 (18)	0.1897 (20)	0.3585 (26)	3.6 (8)
C(44)	0.4872 (20)	0.1396 (22)	0.4872 (25)	4.1 (8)

[a] Esd's are given in parentheses.

Table II. Interatomic Distances of **1** (Å)[a]

Os(1)–Os(2)	3.016 (1)	C(43)–Os(1)	2.965 (25)
Os(1)–Os(3)	2.763 (1)	C(43)–Os(2)	2.198 (26)
Os(2)–Os(3)	2.858 (1)	C(43)–Os(3)	2.263 (27)
Os(1)–C(11)	1.884 (24)	C(11)–O(11)	1.162 (32)
Os(1)–C(12)	1.987 (27)	C(12)–O(12)	1.157 (35)
Os(1)–C(13)	1.902 (26)	C(13)–O(13)	1.153 (33)
Os(2)–C(21)	1.939 (29)	C(21)–O(21)	1.114 (36)
Os(2)–C(22)	2.000 (26)	C(22)–O(22)	1.071 (34)
Os(2)–C(23)	1.961 (28)	C(23)–O(23)	1.062 (37)
Os(3)–C(31)	1.927 (23)	C(31)–O(31)	1.116 (30)
Os(3)–C(32)	1.866 (25)	C(32)–O(32)	1.198 (33)
Os(3)–C(33)	1.912 (32)	C(33)–O(33)	1.132 (39)
C(42)–Os(1)	2.067 (24)	C(41)–C(42)	1.513 (38)
C(42)–Os(2)	2.980 (27)	C(42)–C(43)	1.434 (36)
C(42)–Os(3)	2.364 (28)	C(43)–C(44)	1.436 (35)

[a] Esd's are given in parentheses.

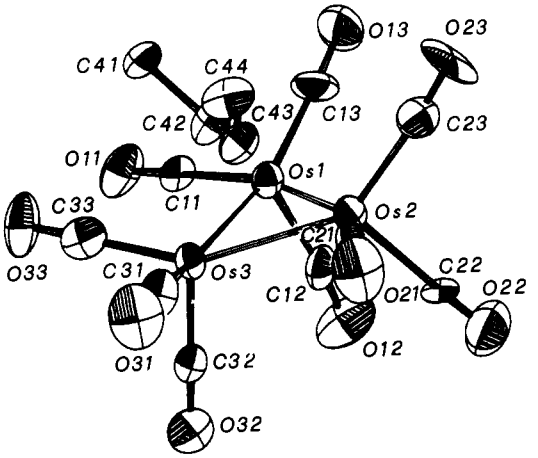

Figure 1. ORTEP view of $H_2Os_3(CO)_9(CH_3C_2CH_3)$ (**1**) (hydrogens not indicated).

(18) (a) Aime, S.; Jannon, G.; Osella, D.; Arce, J.; Deeming, A. J. *J. Chem. Soc., Dalton Trans.* **1984**, 1987. (b) Castiglioni, M.; Milone, L.; Osella, D.; Vaglio, G. A.; Valle, M. *Inorg. Chem.* **1976**, *15*, 394.
(19) Tondello, E. *Inorg. Chim. Acta* **1974**, *11*, L5.
(20) Pople, J. A.; Segal, G. A. *J. Chem. Phys.* **1966**, *44*, 3289.
(21) Mulliken, R. S. *J. Chem. Phys.* **1955**, *23*, 1833.
(22) Löwdin, P. O. *J. Chem. Phys.* **1950**, *18*, 365.

Table III. Bond Angles of **1** (deg)[a]

Os(2)–Os(1)–Os(3)	59.07 (0.04)	Os(1)–Os(3)–C(33)	97.2 (0.8)
Os(1)–Os(2)–Os(3)	56.06 (0.04)	Os(2)–Os(3)–C(31)	98.2 (0.7)
Os(2)–Os(3)–Os(1)	64.87 (0.04)	Os(2)–Os(3)–C(32)	109.6 (0.6)
Os(2)–Os(1)–C(11)	153.1 (0.6)	Os(2)–Os(3)–C(33)	152.0 (0.8)
Os(2)–Os(1)–C(12)	97.0 (0.6)	C(31)–Os(3)–C(32)	99.4 (1.0)
Os(2)–Os(1)–C(13)	109.2 (0.8)	C(31)–Os(3)–C(33)	94.3 (1.0)
Os(3)–Os(1)–C(11)	94.6 (0.6)	C(32)–Os(3)–C(33)	92.7 (1.0)
Os(3)–Os(1)–C(12)	104.2 (0.8)	C(42)–Os(1)–Os(2)	68.9 (0.6)
Os(3)–Os(1)–C(13)	154.1 (0.8)	C(42)–Os(1)–Os(3)	56.4 (0.7)
C(11)–Os(1)–C(12)	95.0 (0.9)	C(42)–Os(3)–Os(1)	46.8 (0.5)
C(11)–Os(1)–C(13)	92.3 (1.0)	C(42)–Os(3)–Os(2)	68.8 (0.5)
C(12)–Os(1)–C(13)	100.0 (1.1)	C(43)–Os(2)–Os(1)	67.2 (0.6)
Os(1)–Os(2)–C(21)	152.9 (0.6)	C(43)–Os(2)–Os(3)	51.2 (0.6)
Os(1)–Os(2)–C(22)	105.6 (0.8)	C(43)–Os(3)–Os(1)	71.5 (0.6)
Os(1)–Os(2)–C(23)	105.1 (0.7)	C(43)–Os(3)–Os(2)	49.1 (0.6)
Os(3)–Os(2)–C(21)	97.6 (0.6)	C(41)–C(42)–C(43)	116.8 (2.2)
Os(3)–Os(2)–C(22)	118.6 (0.6)	C(42)–C(43)–C(44)	126.9 (2.4)
Os(3)–Os(2)–C(23)	142.4 (0.7)	Os(1)–C(42)–Os(2)	70.8 (0.7)
C(21)–Os(2)–C(22)	92.2 (1.1)	Os(1)–C(42)–Os(3)	76.8 (0.8)
C(21)–Os(2)–C(23)	92.5 (1.0)	Os(2)–C(42)–Os(3)	63.4 (0.7)
C(22)–Os(2)–C(23)	97.0 (1.0)	Os(1)–C(43)–Os(2)	69.7 (0.6)
Os(1)–Os(3)–C(31)	160.4 (0.7)	Os(1)–C(43)–Os(3)	62.1 (0.8)
Os(1)–Os(3)–C(32)	95.8 (0.6)	Os(2)–C(43)–Os(3)	79.7 (0.7)

[a] Esd's are given in parentheses.

SHELX[24] and ORTEP[25] programs were used. Final coordinates are reported in Table I.

Results and Discussion

Crystal Structure of 1. An ORTEP view of **1** with the atom-numbering scheme is given in Figure 1; selected bond distances and angles are reported in Tables II and III. Two X-ray structural studies on the related compounds $H_2Ru_3(CO)_9(MeC_2OMe)$ and $H_2Os_3(CO)_9(C_6H_4)$ (benzyne ligand) have already been reported.[26,27]

The three metal atoms give rise to a triangle with dimensions very similar to those reported previously.[26,27] We agree with the suggestion proposed by Farrugia et al.[28] that the large Os(1)–Os(2) distance is determined by the steric requirements of the bridging alkyne rather than by the presence of the hydride bridging the corresponding edge (recently located in the structural determination of $H_2Ru_3(CO)_9(MeC_2OMe)$[26]). On the other hand, the less pronounced lengthening effect of the bridging hydride is best seen by comparing the Os(1)–Os(3) and Os(2)–Os(3) bond distances. The alkyne CH_3–C_2–CH_3 deviates slightly from planarity (torsion angle −10.6 (2.0)°), the maximum deviation from the best plane being 0.04 (2) Å; this plane is nearly perpendicular to the trimetallic plane, the bending angle being 85.6 (3)°. The two lines through the C(42)–C(43) and Os(1)–Os(2) bonds are nearly parallel, with an angle of 8.0 (4)°. This value justifies the "parallel" nomenclature adopted for such type of alkyne coordination mode. The organic moiety is coordinated to the cluster by means of two shorter bonds (Os(1)–C(42) and Os(2)–C(43)) and two larger bond contacts (Os(3)–C(43) and Os(3)–C(42)). These structural parameters have suggested the presence of two σ-type Os(1,2)–C bonds and a further π-type Os(3)–alkyne bond. The nature of such interactions will be discussed in detail in the following by means of the CNDO quantum-mechanical calculations.

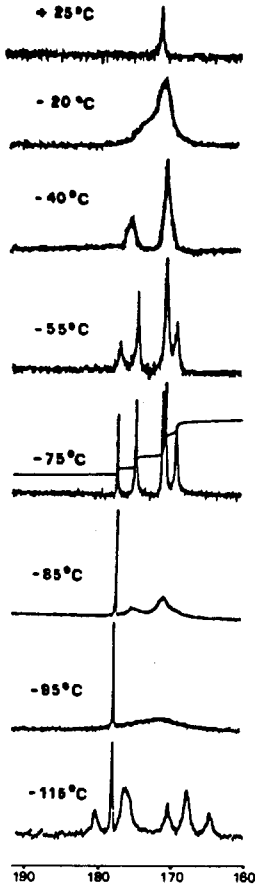

Figure 2. VT $^{13}C\{^1H\}$ NMR spectra of a ^{13}CO-enriched sample of **1**.

Interestingly, the Os_1–Os_2–C_{43}–C_{42} frame is quite asymmetric, with Os(1)–C(42) shorter than Os(2)–C(43), regardless of the type of alkyne substituent.[26,27] In the most recent crystallographic characterization,[26] it has been proposed that the observed distortion is a consequence of the charge imbalance among the metallic centers since no significant asymmetry has been observed in $M_3(\mu_3\text{-}\eta^2\text{-alkyne})$ systems not containing bridging hydrides, provided that the EAN formalism at each metal atom has been satisfied. This argument is further discussed below.

No attempt was made to locate the cluster-bonded hydrogen atoms. On the basis of the recently reported data for the analogous Ru derivative,[26] we will assume that H_a bridges Os(1)–Os(2) while H_b bridges Os(2)–Os(3). In particular, we believe that H_b lies out of the metallic plane opposite to the alkyne side since the Os–Os–CO angles for the axial carbonyls adjacent to this edge (Table III) are significantly wider than the corresponding angles found for the equatorial ones and for the other two edges, following earlier assignments based on the same criteria.[29] We believe H_a to lie in the trimetallic plane, as indicated by molecular models.

^1H and ^{13}C NMR Studies. In the low-field region (not shown here) the ^{13}C NMR spectrum of **1** contains two resonances for the coordinated alkyne (128.7 ppm, quartet, $^2J_{C,H}$ = 5.6 Hz; 35.8 ppm, quartet, $^1J_{C,H}$ = 126.7 Hz), which remain unchanged in the temperature range from −60 to +25 °C. The decreased solubility of this compound prevented examination of spectra at lower temperatures (natural abundance ^{13}C). The VT ^1H NMR spectra confirm the previously reported results:[17] two hydride resonances at low temperature (−50 °C), which merge into a single peak at +40 °C (ΔG^*_{273} = 11.3 kcal/mol); the two methyl groups give a single absorption also at −92 °C.

The VT $^{13}C\{^1H\}$ NMR spectra of a ^{13}CO-enriched sample of **1** are reported in Figure 2. At the lowest achievable temperature (−115 °C, in a Freon-11/CD_2Cl_2 3:1 mixture) the resonances are quite broadened, but the observed pattern accounts for nine

(23) *International Tables for X-ray Crystallography*, 2nd ed.; Kynoch: Birmingham, England, 1974.
(24) Sheldrick, G. M. "SHELX, a Program for Crystal Structure Determination"; University of Cambridge, London, 1976.
(25) Johnson, C. K. "ORTEP-II: A Fortran Thermal-Ellipsoid Plot Program for Crystal Structure Illustration", Oak Ridge National Laboratory, Oak Ridge, TN, 1976.
(26) Churchill, M. R.; Fettinger, J. C.; Keister, J. B.; See, R. F.; Ziller, J. W. *Organometallics* **1985**, *4*, 2112.
(27) Goudsmith, R. J.; Johnson, B. F. G.; Lewis, J.; Raithby, P. R.; Rosales, M. J. *J. Chem. Soc., Dalton Trans.* **1983**, 2257.
(28) Farrugia, L. J.; Howard, J. A. K.; Mitrprachachon, P.; Stone, F. G. A.; Woodward, P. *J. Chem. Soc., Dalton Trans.* **1981**, 162.
(29) Teller, R. G.; Bau, R. *Struct. Bonding (Berlin)* **1981**, *44*, 1.

Table IV. $\Delta G^{\ddagger}$ (kcal/mol) for H_a/H_b Exchange Obtained from VT ^1H NMR Spectra

compd	$\Delta G^{\ddagger}$
$H_2Os_3(CO)_9(MeC_2Me)$ (1)	11.3 (±0.2)
$H_2Ru_3(CO)_9(MeC_2Me)$ (2)	11.3 (±0.2)
$H_2Ru_3(CO)_9(MeC_2Et)$ (3)	11.0 (±0.2)
$H_2Ru_3(CO)_9(EtC_2Et)$ (4)	11.7 (±0.2)
$H_2Ru_3(CO)_9(MeC_2Pr)$ (5)	11.5 (±0.2)

carbonyls as expected from the solid-state structure (180.1 (1), 177.6 (1), 175.7 (3), 170.2 (1), 167.5 (2), and 164.3 (1) ppm, respectively). As the temperature is raised, all the resonances (except that centered at 177.6 ppm) broaden, disappear in the base line, and merge (at −75 °C) into four absorptions of relative intensity 2.

The mechanism suggested by Lewis[30] and Deeming[17] implies that the average of the carbonyls to a 1:2:2:2:2 pattern (as observed at −75 °C) is caused by the transfer of H_b across the two Os(1)–Os(3) and Os(2)–Os(3) edges, whereas all the remainder of the molecule is static. However, from the X-ray structure, we know that the asymmetry in the molecule is not induced only by H_b but also by the rather asymmetric coordination mode of the alkyne moiety; it follows, then, that this source of asymmetry is also averaged by the dynamic behavior. Therefore, the following concerted motion is suggested:

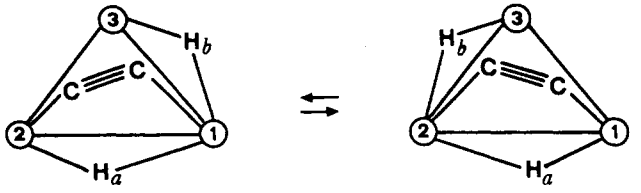

This motion gives rise to an effective mirror plane perpendicular to the metallic triangle, and noteworthy, the single carbonyl group that lies on this plane (viz. the axial CO at the Os(3) center) appears as a sharp singlet throughout. The $\Delta G^{\ddagger}_{273}$ for this process has been estimated as 7.4 kcal/mol. The low energy involved in this process does not allow the splitting of the two ^1H methyl resonances also at −92 °C since the expected difference in their chemical shifts is noticeably smaller than the separation (in hertz) observed with each pair of carbonyl groups.

Further analysis of the VT ^{13}C NMR spectra shows that at −40 °C the peaks at 177.6 and 169.1 ppm are more broadened than the others and, as the temperature is increased, they disappear in the base line. Tentatively, these resonances are assigned to axial and equatorial carbonyls on Os(3); it follows that the localized CO exchange at this $Os(CO)_3$ unit requires a lower activation energy than that needed for CO scrambling at the other two osmium centers.

We then examined the VT ^1H and ^{13}C NMR spectra of the analogous Ru derivative **2**. The general features observed both in ^{13}C and ^1H spectra are very similar to those already discussed for **1**. Actually (see Table IV) the activation energy for H_a/H_b exchange is quite similar in a series of derivatives that we have considered: this observation contrasts with the previous report,[7b] which suggested a marked influence on this exchange process from the nature of the substituents on the alkyne ligand. The ^{13}C spectrum of **2** indicates that at −105 °C the effective mirror plane perpendicular to the Ru_3 triangle created by hydride movement from the 2,3 edge to the 1,3 edge is still maintained (five signals are in fact observed at 200.0 (1), 193.7 (2), 191.4 (2), 191.3 (2), and 190.6 (2) ppm, respectively).

The VT ^1H and ^{13}C NMR spectra of **3** were then considered. The ^{13}C spectrum at −92 °C (see Figure 3) shows eight resonances at 198.9, 194.0, 191.8, 191.3, 191.1, 189.4, 188.6, and 187.7 ppm in the relative intensity ratio of 1:1:1:2:1:1:1:1, respectively. As the temperature is increased, three resonances (198.9, 191.1, and 187.7 ppm) broaden and collapse in the base line; finally, at −24 °C, all the resonances are broadened and a single averaged resonance is observed at room temperature. This behavior clearly parallels that one described for **1** and **2** at temperatures above −70 °C, but in **3** the asymmetric substitution on the alkyne is responsible for the almost complete differentiation of the nine structurally different carbonyls (two of them are overlapped at −92 °C). An insight into the relationship of the carbonyl groups and cluster-bonded hydrogen atoms arises from the observation of the proton-coupled ^{13}C spectrum at −92 °C. This shows that only three resonances [191.8 ppm ($^2J_{C,H}$ = 9.2 Hz); 189.4 ppm ($^2J_{C,H}$ = 2.0 Hz); 188.6 ppm ($^2J_{C,H}$ = 11.5 Hz)] are split by hydrogen. Selective decoupling experiments proved that the C,H couplings disappear when irradiation is carried out on the hydride at −18.4 ppm, which is then assigned to H_a on the basis of the observed C,H coupling pattern. Since no $^2J_{C,H}$ was detected in the ^{13}C spectra of **1** and **2** as well as no H,C coupling for any of the three carbonyls on Ru(3) (assigned from their dynamic behavior) of **3**, we think that the observed $^{13}C,^1H$ coupling pattern has to be associated with a remarkable change in the H_a position on going from the symmetrically substituted alkyne derivatives **1** and **2** to the asymmetrically substituted complex **3**.

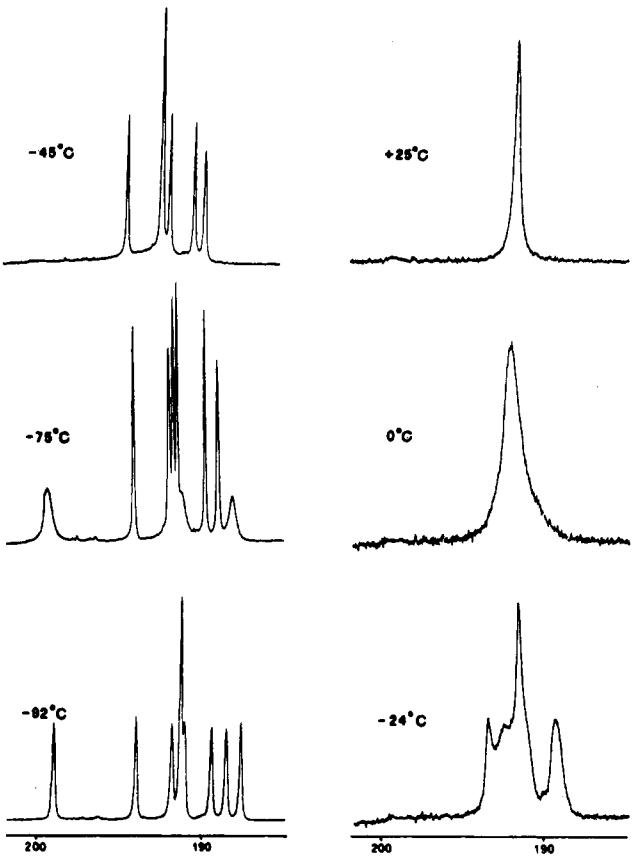

Figure 3. VT $^{13}C\{^1H\}$ NMR spectra of a ^{13}CO-enriched sample of **3**.

This behavior was further confirmed by considering the inseparable mixture of **4** and **5**. The ^{13}C NMR spectrum of the CO region at −92 °C was not immediately understandable since it showed a number of overlapped signals, but comparison of their VT behavior with that of **3** finally allowed a complete assignment of the ^{13}CO resonances of each isomer **4**: 199.0 (1), 192.5 (2), 190.2 (4), 189.3 ppm (2). **5**: 189.9 (1), 194.2 (1), 192.2 (1), 191.5 (1), 191.4 (1), 191.0 (1), 189.3 (1), 188.3 (1), 187.3 ppm (1). The dynamic behavior, in the range of temperatures from −90 to +25 °C, follows the same path found for **3**. The important point was that, at −90 °C, only three resonances assigned to isomer **5** were affected by proton coupling with H_a to the same extent as already observed for **3** whereas isomer **4** behaves as **2**. These observations support the view that the minor charge difference caused by the different alkyl substituents on the acetylenic carbons is enough to affect the steric relationship between H_a and a set of distinct carbonyl groups.

(30) Evans, J.; Johnson, B. F. G.; Lewis, J.; Matheson, T. W. *J. Organomet. Chem.* **1975**, *97*, C16.

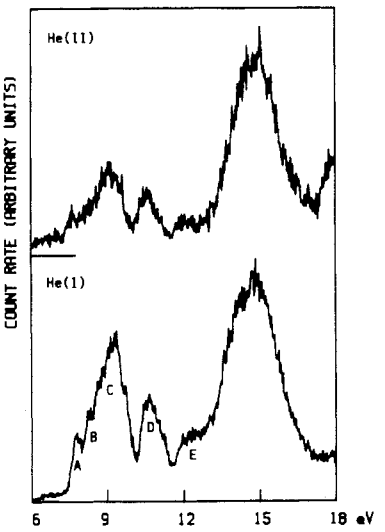

Figure 4. He I and He II excited PE spectra of **1**.

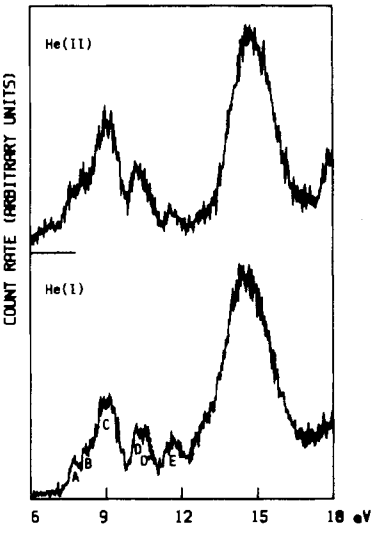

Figure 5. He I and He II excited PE spectra of **2**.

Table V. Ionization Energy Data (eV) for the Compounds **1** and **2**

band	1	2	band	1	2
A	7.82	7.73	D	10.66	10.25
B	8.30	8.30	D′		10.64
C	9.32	9.12	E	12.15	11.60

UV-PE and CNDO Results. The He I and He II excited PE spectra of **1** and **2**, with bands alphabetically labeled, are reported in Figures 4 and 5. The pertinent IE values are reported in Table V.

The observed IE range, according to previous data on related organometallic carbonyl clusters,[4,31] can be divided into two distinct regions, 7.5–13 and 13–18 eV. In the first region ionizations from *n*d metal-based MOs having metal–metal bonding and nonbonding character are usually found together with ionizations from MOs mainly localized on the organic portion of the molecule and representing cluster–substrate bonding interactions. In the second region, usually too complex for detailed assignments, are found ionizations of the carbonyl MOs (related to the 5σ, 1π, and 4σ MOs in free CO) and of the inner levels of the organic substrates. The region 7.5–13 eV is, then, the most suitable for discussing the bonding of the alkyne over the metallic triangle.

Turning to Figures 4 and 5, by analogy with other similar clusters,[4,31] we assign band A to the ionization from a M–M bonding MO. Bands B and C are related to ionizations from MOs largely localized on the metal atoms with predominant nonbonding *n*d character, referenced as "t_{2g}-like" because of their parentage with pseudo-t_{2g} orbitals of a $M(CO)_4$[32] fragment. As previously shown,[4,31] the ionizations within the t_{2g}-like set can span 1.5–2 eV so that some stabilized components contribute also to the higher IE band D. On the other hand, we expect that band D also contains ionizations from some alkyne–cluster bonding MO. The subsequent broad band E we assume to be related to inner alkyne–cluster bonding levels together with the σ(C–C) and σ(C–H) levels of the organic ligand. As far as the metal–hydride ionizations are concerned, reference to previous PE data[4,31] suggests that they must be also included under either band D or band E.

The inspection of the He II spectra confirms the above qualitative assignments; in particular, band E exhibits a considerable intensity decrease with respect to the lower IE bands, in agreement with the intensity variations expected for C_{2p}-based MOs with respect to M_{nd}-based MOs on switching from He I to He II radiation.[33] Moreover, band D, which is resolved into two components (D and D′) in the case of **2**, shows an intensity decrease of the higher IE D′ component, demonstrating the presence of d-based and ligand-based ionizations under the same envelope.

A more detailed discussion of the nature of the MOs that give rise to the above UV-PE spectral pattern will be accomplished by using quantum-mechanical calculations. CNDO eigenvalues and eigenvectors of the 15 outermost MOs of $H_2Ru_3(CO)_9(HC_2H)$[34] are reported in Table VI. The CNDO results provide an eigenvalue spectrum (within Koopmans' theorem[35]) that is in general agreement with the reported PE data. The limitations of the semiempirical approach and the molecular complexity do not allow, however, a direct one-by-one matching between the theoretical and the experimental PE data.

The HOMO (63) (Table VI) is associated with Ru(1)–Ru(3) bonding character, related to one of the "e_g-like" M–M bonding MOs of $M_3(CO)_{12}$.[36] This MO must be related to band A. The eigenvector analysis of the subsequent MOs shows that there is no distinct Ru(1)–Ru(2) and Ru(2)–Ru(3) bonding MO since the interaction with the bridging hydrides weakens the direct metal–metal bond.[31] As a consequence, the parent Ru(1)–Ru(2) and Ru(2)–Ru(3) MOs are shifted toward higher IEs and lie in the same energy region of the following t_{2g}-like nine orbitals (60-52), which are largely localized on the metallic centers with some mixing with carbonyl $2\pi^*$ MOs. The corresponding ionizations give rise to bands B, C, and D, the experimental B–D splitting being theoretically well reproduced by the energy difference between MOs 51 and 62. Within this set of MOs, the three innermost MOs (53–51) present the largest involvement of the bridging hydrides. Both MOs 51 and 52 also contain Ru(1)–C(42) and Ru(2)–C(43) bonding character. These MOs represent the interaction between the π^* MO of the alkyne fragment, whose lobes point toward the two metallic sites, and the suitable out-of-plane component of the 2e MO of the $M_3(CO)_9$ fragment.[9] This indicates a strong cluster→alkyne back-bonding interaction, activating the organic fragment, similar to that already found in the related **B** type iron cluster.[4b] On the basis of the reported He I/He II behavior of the spectrum of **2**, we propose to assign shoulder D′ to the ionization from the MO 51.

The next two MOs (50, 49) describe cluster–alkyne bonding levels having a parentage with the alkyne occupied π orbitals. Actually, they are mainly localized on the alkyne and are both

(31) (a) Granozzi, G.; Tondello, E.; Ajó, D.; Casarin, M.; Aime, S.; Osella, D. *Inorg. Chem.* **1982**, *21*, 1081. (b) Granozzi, G.; Benoni, R.; Tondello, E.; Casarin, M.; Aime, S.; Osella, D. *Inorg. Chem.* **1983**, *22*, 3899. (c) Granozzi, G.; Benoni, R.; Acampora, M.; Aime, S.; Osella, D. *Inorg. Chim. Acta* **1984**, *84*, 95. (d) Chesky, P. T.; Hall, M. B. *Inorg. Chem.* **1983**, *22*, 3327, and previous papers of the series.
(32) Elian, M.; Hoffmann, R. *Inorg. Chem.* **1975**, *14*, 1058.
(33) (a) Gelius, U. In *Electron Spectroscopy*; Shirley, D. A., Ed.; North-Holland: Amsterdam, 1972; pp 311–334. (b) Schweig, A.; Thiel, W. *J. Electron Spectrosc. Relat. Phenom.* **1974**, *3*, 27; *J. Chem. Phys.* **1974**, *60*, 951.
(34) Assuming geometrical parameters from ref. 26.
(35) Koopmans, T. C. *Physica (Amsterdam)* **1933**, *1*, 104.
(36) Ajó, D.; Granozzi, G.; Tondello, E.; Fragalá, I. *Inorg. Chim. Acta* **1979**, *37*, 191.

Table VI. CNDO Results for $H_2Ru_3(CO)_9(HC_2H)$[a]

		% population									
		Ru									
MO	eigenvalue, eV	Ru(1)	Ru(2)	Ru(3)	H_a	H_b	C(42)	C(43)	H(42)	H(43)	9 CO
63 (HOMO)	−7.05	38	6	41			2	2		1	10
62	−8.28	23	25	26	6	3	6	3		2	6
61	−8.60	26	22	31	2		7	2	2		8
60	−8.86	41	3	46			1				9
59	−9.00	65	8	10		1	1	2		2	11
58	−9.12	2	21	63		1	2	1			10
57	−9.23	35	30	22							13
56	−9.28	40	34	12			1	2	1		10
55	−9.47	3	76	7	1		1	1	2		9
54	−9.70	10	43	28	4	3					12
53	−10.07	27	43	4	12						14
52	−10.34	9	27	32	4	6	5	2	3	1	11
51	−10.91	23	13	21	1	11	3	12	3	5	8
50	−13.09	10	8	5			27	34	3	1	12
49	−13.36	6	10	9		1	30	25		2	17

[a] Geometrical parameters from ref 26.

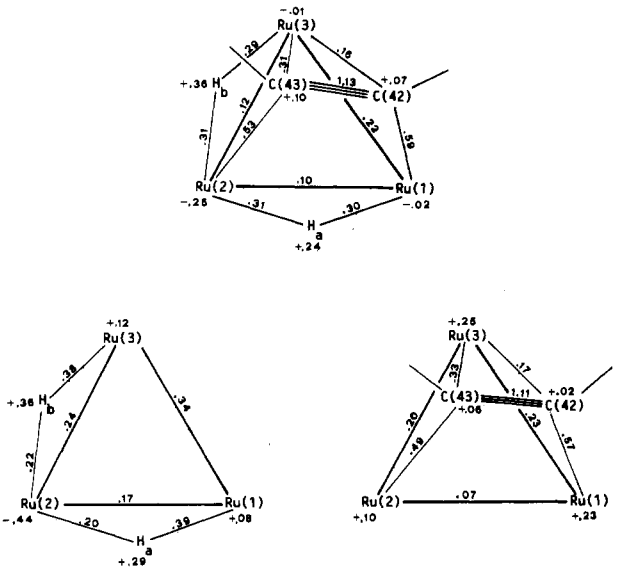

Figure 6. CNDO gross atomic charges and overlap populations of $H_2Ru_3(CO)_9(HC_2H)$, $H_2Ru_3(CO)_9$, and $Ru_3(CO)_9(HC_2H)$.

C(42)–C(43) bonding in character (see Table VI). Between them, the inner one contributes to a larger extent to the Ru(3)–alkyne interaction.

The electronic density distribution and bond strengths can be conveniently discussed by reference to Figure 6, where the CNDO gross atomic charges and overlap populations (OPs) are reported for the studied cluster and for its constituent fragments (adopting the same geometry of the cluster). Looking at the gross atomic charges of the metal atoms of the cluster, we find that the qualitative prediction based on the EAN rule (Ru(1) 17.5 e, Ru(2) 18 e, Ru(3) 18.5 e) is not fulfilled because two factors: (i) the existence of back-bonding interactions that are neglected in the EAN formalism and (ii) the distorted geometrical arrangement of the alkyne over the metallic triangle. The Ru(2) atom is particularly electron-rich owing to the polarizing effect of the two bridging hydrides (compare in Figure 6 the gross atomic charges in $H_2Ru_3(CO)_9$ and $Ru_3(CO)_9(HC_2H)$). In our opinion, the large charge imbalance between Ru(1) and Ru(2) is the driving force for the distortion of the alkyne coordination.

The metal–metal OPs are consistent with the existence of one strong (Ru(1)–Ru(3)) and two weak M–M interactions. As far as the small Ru(1)–Ru(2) OP value (0.10 e) is concerned, a CNDO calculation performed on the $Ru_3(CO)_9$ fragment, adopting the same geometry of the cluster, shows a Ru(1)–Ru(2) OP value of 0.34 e; thus, the strong reduction of the Ru(1)–Ru(2) OP can be mostly ascribed to the electronic perturbation induced by the coordinated alkyne whereas H_a plays a minor role (Figure 6). On the other hand, both the alkyne and H_b contribute to a similar extent to the weakening of the Ru(2)–Ru(3) bond (see Figure 6). Regarding activation of the alkyne ligand, a CNDO calculation on the "free" HC≡CH unit (adopting the same geometry as in the cluster) reveals a remarkable increase of the C–C OP (1.40 vs. 1.13 e in the organometallic compound). We ascribe this large OP reduction to an extensive rehybridization of carbon atoms due to π and π^* orbital involvement in the alkyne–cluster interaction. Final considerations concern the Ru(1)–C(42), Ru(2)–C(43), and the alkyne–Ru(3) OPs: from Figure 6 it is clearly seen that their values are consistent with two strong σ-type and one weaker π-type interactions.

Theoretical Considerations on Coordination Modes B and C. An exhaustive discussion on the frontier orbital interactions that favor mode **B** over **C** in 46-e clusters has been already reported by Schilling and Hoffmann.[9,16] Nothing has been proposed however about the reasons that lead to a 46-e unsaturated cluster for Fe in contrast to 48-e saturated clusters for Ru and Os. With the aim at clarifying this point, we have carried out a series of CNDO calculations on symmetric models of both **B** and **C** arrangements for the Fe and Ru compounds of general formula $M_3(CO)_9(HC_2H)$ (46-e clusters).[37]

The MO energy sequences and compositions resulting from these calculations agree, with minor differences, with those of Schilling and Hoffmann.[9] In particular, our calculations confirm the existence of a low-lying LUMO in coordination mode **C**. This argument has been invoked to explain the preference for **C** in a 48-e saturated cluster.[9] Moreover, within geometry **C**, our results indicate that the LUMO is lower lying in the ruthenium compound (+0.65 eV) than in the iron analogue (+1.89 eV). This concurs with the preference for a 48-e situation in triruthenium cluster complexes.

On the other hand, from the Mulliken population analysis shown in Figure 7 it emerges that another driving force, i.e. the charge equilibration within the metallic framework, could explain the preference of coordination mode on changing the metal atoms. Actually, the gross atomic charges of the three Fe atoms in arrangement **B** (Fe +0.52 e, Fe′ +0.55 e) show a better charge equilibration than those in **C** (Fe +0.52 e, Fe′ +0.70 e) while the opposite is true for the Ru analogues, where **C** (Ru +0.27 e, Ru′ +0.30 e) shows a better charge equilibration than **B** (Ru +0.17 e, Ru′ +0.27 e). These results, in our opinion, depend on the different electronegativities of iron and ruthenium atoms (Pauling

(37) The **C** iron geometry has been obtained from the known structure of **B**[5] through a 90° rotation of the alkyne about the axis perpendicular to the metallic plane and a shift of the alkyne moiety in order to adjust the Fe–C distance as in **B**. The **B** geometry of Ru has been similarly obtained from the X-ray structural parameters of the corresponding **C** compound.[26]

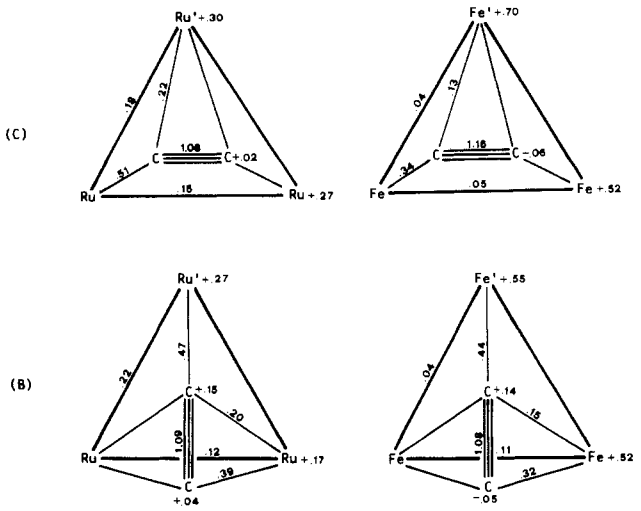

Figure 7. CNDO gross atomic charges and overlap populations of **B** and **C** models of $M_3(CO)_9(HC_2H)$ (M = Fe, Ru) complexes.

values, 1.8 vs. 2.2), which modify the balance between the alkyne–cluster donation/back-donation. In fact, the charge equilibration inside the trimetallic ring in coordination mode **B** for the Fe_3–alkyne complex can be explained by a strong back-donation from the two symmetry-equivalent Fe atoms.[4b,c] On the contrary, in the hypothetical coordination mode **B** for the Ru_3 analogue, the back-donation is not so effective and the charge equilibration is far from being reached; actually, the two equivalent Ru atoms are less positively charged than the unique Ru′ atom (see Figure 7). On the other hand, a comparison between the Fe and Ru **C** arrangements (Figure 7) shows that the donation from the alkyne toward the unique metal atom M′ is more effective for the Ru than for the Fe compound (larger M′–alkyne OP when M′ = Ru). Furthermore, the reduced aptitude of Ru atoms to back-donate is overriden by the favorable geometrical arrangement (compare the Ru atomic charges in **B** and **C**).[38]

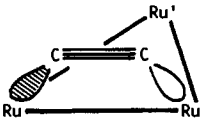

These results suggest that coordination mode **C** could already be favored for a 46-e Ru_3–alkyne compound; the consequent low-lying LUMO would then produce the acquisition of two more electrons in order to reach the 48-e saturated configuration.

Acknowledgments. Thanks are expressed to the Ministero della Pubblica Istruzione (Grant MPI 12/2/15) and to the CNR of Rome for generous financial support of this study. We also thank Johnson-Matthey Ltd. for a loan of $RuCl_3$ and OsO_4. The assistance of a reviewer is acknowledged in the interpretation of the NMR results.

Registry No. **1**, 57373-23-6; **2**, 80303-38-4; **3**, 56943-12-5; **4**, 80303-37-3; **5**, 98797-97-8.

Supplementary Material Available: A table of anisotropic thermal parameters for $H_2Os_3(CO)_9(CH_3C_2CH_3)$ (1 page); a table of structure factor amplitudes for $H_2Os_3(CO)_9(CH_3C_2CH_3)$ (12 pages). Ordering information is given on any current masthead page.

(38) A similar bonding scheme has been invoked for the μ_4-η^2 coordination mode **D** of the alkyne in a "butterfly" cluster; actually, the **C** arrangement can be regarded as a portion of a **D** arrangement where a "wing" metal atom has been lost.

Contribution from the Department of Chemistry, University of South Carolina, Columbia, South Carolina 29208

Ligand Substitution vs. Ligand Addition. 2. Reaction of Dimethylamine with $Ru_3(CO)_9(\mu_3\text{-}S)_2$ and the Crystal and Molecular Structures of $Ru_3(CO)_7(NHMe_2)(\mu\text{-}Me_2NC{=}O)(\mu_3\text{-}S)_2(\mu\text{-}H)$ and $Ru_3(CO)_6(NHMe_2)(\mu\text{-}Me_2NC{=}O)_2(\mu_3\text{-}S)_2$

Richard D. Adams* and James E. Babin

Received June 2, 1986

The reaction of $Ru_3(CO)_9(\mu_3\text{-}S)_2$ (**1**) with an excess of Me_2NH at 25 °C yields two products, $Ru_3(CO)_7(NHMe_2)(\mu\text{-}Me_2NC{=}O)(\mu_3\text{-}S)_2(\mu\text{-}H)$ (**2**, 64%) and $Ru_3(CO)_6(NHMe_2)(\mu\text{-}Me_2NC{=}O)_2(\mu_3\text{-}S)_2$ (**3**, 20%). Both products were characterized by IR and ^1H NMR spectroscopy and elemental and single-crystal X-ray diffraction analyses. For **2**: space group $P2_1/c$, a = 14.003 (2) Å, b = 9.534 (1) Å, c = 17.061 (2) Å, β = 111.91 (1)°, Z = 4, ρ_{calcd} = 2.14 g/cm³. The structure was solved by direct methods and was refined (2816 reflections) to the final values of the residuals R = 0.0373 and R_w = 0.0438. The structure consists of an open cluster of three metal atoms with two triply bridging sulfido ligands and a C,O-bonded *N,N*-dimethylcarbamoyl ligand bridging an unbonded pair of ruthenium atoms. For **3**: space group $P2_1/c$, a = 18.030 (3) Å, b = 9.148 (2) Å, c = 14.397 (4) Å, β = 90.07 (2)°, Z = 4, ρ_{calcd} = 2.03 g/cm³. The structure was solved by direct methods and was refined (1909 reflections) to the final values of the residuals R = 0.0497 and R_w = 0.0488. The structure of **3** consists of an open cluster of three metal atoms with only one Ru–Ru bond. There are two triply bridging sulfido ligands, and two *N,N*-dimethylcarbamoyl ligands that bridge both nonbonded Ru–Ru interactions. An intermediate formulated as $Ru_3(CO)_8(NHMe_2)(\mu_3\text{-}S)_2$ was observed spectroscopically when Me_2NH was added to **1** slowly. Reaction of **2** with CO yields $Ru_3(CO)_8(\mu\text{-}Me_2NC{=}O)(\mu_3\text{-}S)_2(\mu\text{-}H)$.

Introduction

Comparitively few studies have been focused on the reactivity of homologous series of transition-metal cluster compounds.[1] In part 1 of this series we reported the results of our studies of the reactions of dimethylamine with the sulfur-bridged trinuclear clusters $M_3(CO)_9(\mu_3\text{-}S)_2$ (M = Fe and Os).[2] It was observed that the iron compound reacted exclusively by a ligand substitution process while the osmium cluster reacted exclusively by an addition reaction, which led to the formation of a bridging carbamoyl ligand that induced the cluster to open. Our studies of the reaction of the third member of this series, $Ru_3(CO)_9(\mu_3\text{-}S)_2$ (**1**), with dimethylamine have now been completed and are described in this report.

Experimental Section

General Procedures. Reactions were performed under a dry nitrogen atmosphere, unless otherwise specified. Reagent grade solvents were

(1) Muetterties, E. L.; Burch, R. R.; Stolzenberg, A. M. *Annu. Rev. Phys. Chem.* **1982**, *33*, 89 and references therein.
(2) Adams, R. D.; Babin, J. E. *Inorg. Chem.* **1986**, *25*, 3418.

0020-1669/86/1325-4010$01.50/0